Applied Catalysis A: General 535 (2017) 77–84

Contents lists available at ScienceDirect

Applied Catalysis A: General

journal homepage: www.elsevier.com/locate/apcata

Aerobic oxidation of alcohols over Ru-Mn-Ce and Ru-Co-Ce catalysts: The effect of calcination temperature

Gui Liu[a], Junhua Liu[a,b,*], Wenxiu Li[a], Cheng Liu[a], Fang Wang[c,*], Junkai He[d], Curtis Guild[d], Jing Jin[d], David Kriz[d], Steven L. Suib[d,*]

[a] College of Chemistry and Materials Science, Nanjing Normal University, Nanjing 210023, China
[b] Jiangsu Collaborative Innovation Center of Biomedical Functional Materials, Jiangsu Key Laboratory of Biomedical Materials, College of Chemistry and Materials Science, Nanjing Normal University, Nanjing 210023, China
[c] College of Chemistry and Molecular Engineering, Nanjing Tech University, Nanjing 210009, China
[d] Department of Chemistry, University of Connecticut, Storrs, CT 06269, USA

ARTICLE INFO

Article history:
Received 26 October 2016
Received in revised form 6 January 2017
Accepted 4 February 2017
Available online 6 February 2017

Keywords:
Aerobic oxidation
Co-precipitation method
Mixed oxides
Oxidation of alcohols

ABSTRACT

Two ternary mixed oxides, Ru-Mn-Ce and Ru-Co-Ce, were prepared by a co-precipitation method and used in the aerobic oxidation of alcohols to corresponding aldehydes (ketones). Interestingly, different catalytic results were obtained when these compounds were calcined. The calcination temperature had an adverse effect on the catalytic performance of Ru-Mn-Ce catalysts, while being beneficial to the Ru-Co-Ce catalysts. To illustrate these effects, these materials were characterized using X-ray diffraction (XRD), Fourier transformed infrared spectroscopy (FT-IR), X-ray photoelectron spectroscopy (XPS), Temperature-programmed reduction (TPR), Electron paramagnetic resonance (EPR) and other techniques. The data showed that ruthenium oxides were uniformly dispersed in the mixed oxides, and phase transformations occur after calcination. Mn_3O_4 was transformed to MnO_2 for the Ru-Mn-Ce catalyst, while CoO(OH) was transformed to Co_3O_4 in the Ru-Co-Ce catalyst. The interactions between ruthenium oxides and Co (Mn)-Ce mixed oxides of the former strengthened while the latter weakened. Calcination decreased the content of adsorbed oxygen and restricted oxygen transfer mechanism in the manganese system, while the opposite effect was observed with the cobalt-containing catalyst. Under optimal reaction conditions, various kinds of alcohols were transformed to corresponding aldehydes (ketones) in high yields over the Ru-Mn-Ce catalyst suggesting these ternary oxides are environmental friendly and economical catalytic systems.

1. Introduction

Selective oxidation of alcohols to aldehydes (ketones) has been considered as one of the most fundamental organic reactions, with the products widely used in the manufacture of perfumes, agricultural chemicals, and other fine chemicals [1–3]. Environmental and economic concerns lead researchers to require clean oxidation procedures that minimize byproducts and wastes, affected by replacing the conventional stoichiometric methods with atom-efficient catalytic protocols using molecular oxygen as the sole oxidant. Recently many outstanding results have been reported using noble metals (Ru, Pd, Au, etc.) as heterogeneous catalysts [3–6]. However, these supported catalysts always face the loss of the noble metals, which is a critical issue for the reusability of catalysts.

Much attention has been given to mixed metal oxides (MMOs), usually prepared by a one-pot synthesis method, e.g. the metal doped vanadium phosphorus mixed oxides (M-VPOs) [7,8] and metal doped molecular sieves [9,10]. In these systems, noble metals are doped into the catalysts directly, forming a uniform compound which minimizes synthesis and loss of the metals. Additionally, noble metals also can be put into catalysts by a co-precipitation method, generally uniform mixed oxide (hydroxide) catalysts. These materials containing noble metals are formed when metal precursor solutions are carefully mixed under vigorous stirring, yielding solid precipitates [11,12]. For aerobic oxidative catalysts, most researchers believe that excellent catalytic performance originates from highly dispersed metal components and rich oxygen storage capacity, surface oxygen vacancies and defects, and some

* Corresponding author.
E-mail addresses: liujh2007@aliyun.com (J. Liu), wangfang2012@njtech.edu.cn (F. Wang), steven.suib@uconn.edu (S.L. Suib).

http://dx.doi.org/10.1016/j.apcata.2017.02.006
0926-860X/

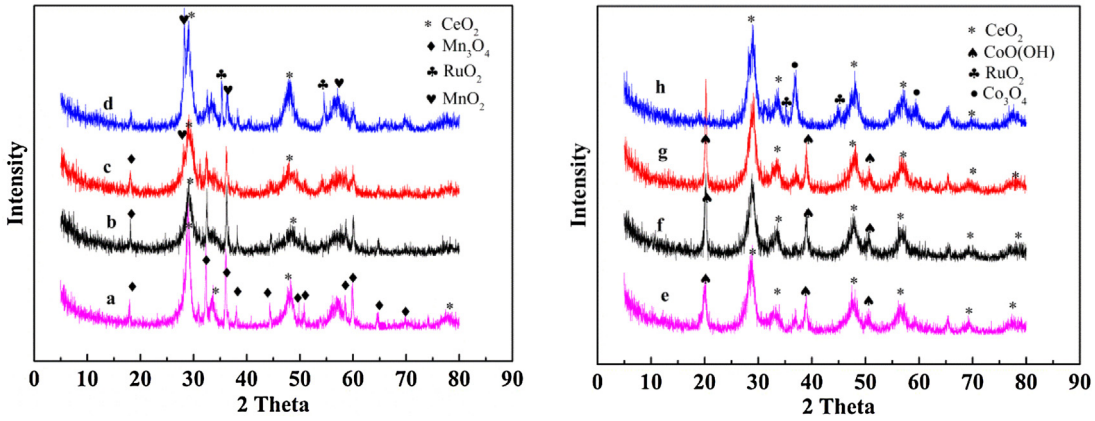

Fig. 1. XRD patterns of catalysts (a) Mn-Ce, (b) Ru-Mn-Ce, (c) Ru-Mn-Ce (300), (d) Ru-Mn-Ce (500) and (e) Co-Ce, (f) Ru-Co-Ce, (g) Ru-Co-Ce (300), (h) Ru-Co-Ce (500).

mixed oxides consisting of cerium oxide, zirconium oxide and iron oxide, have been used for oxidative reactions [13,14].

For MMOs, more active oxygen species can be produced due to the synergistic interaction of different oxides, and they show more excellent catalytic performance than unmixed ones [14,15]. To date, ternary mixed oxides containing noble metals are rarely reported. In this article, Ru-Mn-Ce and Ru-Co-Ce ternary-mixed-oxides were prepared by a co-precipitation method and were investigated as catalysts for aerobic oxidation of alcohols. Interestingly, the calcination temperature has an adverse effect on oxidation of benzyl alcohol over Ru-Mn-Ce catalysts, while being beneficial over the Ru-Co-Ce catalysts.

2. Experimental

2.1. Catalyst preparation

A certain amount of Na_2CO_3 (0.5 M) and NaOH (1.5 M) was slowly dissolved in 30 mL distilled water to produce solution A. Solution B was composed by dissolving 2.2140 g of Ce $(NO_3)_2{\cdot}6H_2O$, 2.5000 g of Mn $(CH_3COO)_2$ (n_{Ce}/n_{Mn} = 0.5) and 0.317 g of $RuCl_3$ in 20 mL distilled water. Solution A was then slowly dripped into solution B under vigorous stirring. The resulting solid product was aged in the mother liquor at room temperature for 24 h, and then the dark brown product was filtered, washed with distilled water, and dried at 110 °C for 10 h to obtain a black powder. The catalysts were calcined at 300 °C and 500 °C, yielding materials referred to hereafter as Ru-Mn-Ce, Ru-Mn-Ce (300) and Ru-Mn-Ce (500), respectively. Ru-Co-Ce catalysts were prepared by a similar procedure with $Co(CH_3COO)_2{\cdot}4H_2O$, the black powders obtained were calcined at 300 °C and 500 °C, which are signed as Ru-Co-Ce, Ru-Co-Ce (300) and Ru-Co-Ce (500), respectively.

2.2. Catalyst characterization

The morphologies of obtained catalysts were examined by transmission electron microscopy (TEM) (FEI Talos F200X) and scanning electron microscopy (SEM) (JSM-7600F). The crystals of the catalysts were studied by X-ray diffraction (XRD) (X'Pert PRO PANalytical). Specific surface area was measured by N_2 adsorption–desorption experiments at 77 K in an ASAP 2010 instrument. The surface composition was determined by X-ray photoelectron spectroscopy (XPS) (VG ESCALAB210) using a K-Alpha-surface analysis system with monochromatized X-Rays. FT-Infrared spectroscopy was performed on a Bruker Tensor 27 spectrometer. Raman spectra were recorded in a dispersive Horiva Jobin Yvon LabRam HR800 Confocal Raman Microscope with a 20 mW green laser (532.14 nm) without a filter and using a 600 grooves/mm grating. Temperature-programmed reduction (TPR) of catalysts was carried out on a Micromeritics 2920 apparatus. Catalyst samples (60 mg) were heated to 800 °C at a rate of 10 °C/min in a H_2-Ar (5:95) gas flow (50 cm^3/min). The electron paramagnetic resonance (EPR) spectra were recorded on a Bruker (EMXNano) spectrometer, all spectra were recorded at a power of 0.3 mW, a modulation amplitude of 4 G, and a modulation frequency of 100 KHz. Inductively coupled plasma optical emission spectroscopy (ICP-OES) analysis was carried out using a Varian 720ES spectrometer.

2.3. Catalytic studies

A typical example for the oxidation of benzyl alcohol by the Ru-Mn-Ce catalyst is as follows: A mixture of catalyst (0.05 g, Ru 0.03 mmol), benzyl alcohol (4 mmol) and benzotrifluoride (5 mL) was stirred in a 100 mL round-bottom flask equipped with a condenser. All reactions were performed under an oxygen atmosphere using an oxygen balloon. The reaction was initiated by immersing the flask in the oil bath kept at the reaction temperature, and then carried out with vigorous stirring for a certain time. Products were analyzed by a standardized gas chromatograph (GC 9560) with a SE-54 capillary column. For recyclability studies, the used catalyst was washed with water, followed by drying at 110 °C, and then subjected to the alcohol oxidation under the same conditions.

3. Results and discussion

3.1. Catalyst characterization

Fig. 1 shows the XRD patterns of Mn-Ce, Co-Ce mixed oxides and corresponding Ru-Mn-Ce and Ru-Co-Ce catalysts calcined at different temperatures. As shown in Fig. 1(a–d), the diffraction peaks at 2θ = 28.6, 33.1, 47.5 and 56.3° could be assigned to CeO_2 (JCPDS: 43-1002), the intensive and sharp diffractions at 2θ= 18.0, 28.9, 31.0, 32.3, 36.1, 36.4, 38.0, 44.4, 50.7, 58.5, 59.8 and 64.7° can be primarily attributed to Mn_3O_4 (JCPDS: 24-0734), the peaks ascribed to the phases of Mn_3O_4 and CeO_2 are obvious and the peaks corresponding to the RuO_2 almost are invisible before the catalysts are calcined. With calcination the peaks corresponding to the Mn_3O_4 are weaker and new peaks assigned to MnO_2 (JCPDS: 50-0866) appear, which indicates that most of the Mn_3O_4 has transformed to MnO_2 after calcination. Meanwhile, the peaks corresponding to RuO_2 (JCPDS: 40-1290) and CeO_2 phases increased with the higher calcined temperature (especially at 500 °C), suggesting the RuO_2 and CeO_2 phases segregate and are isolated with the heat

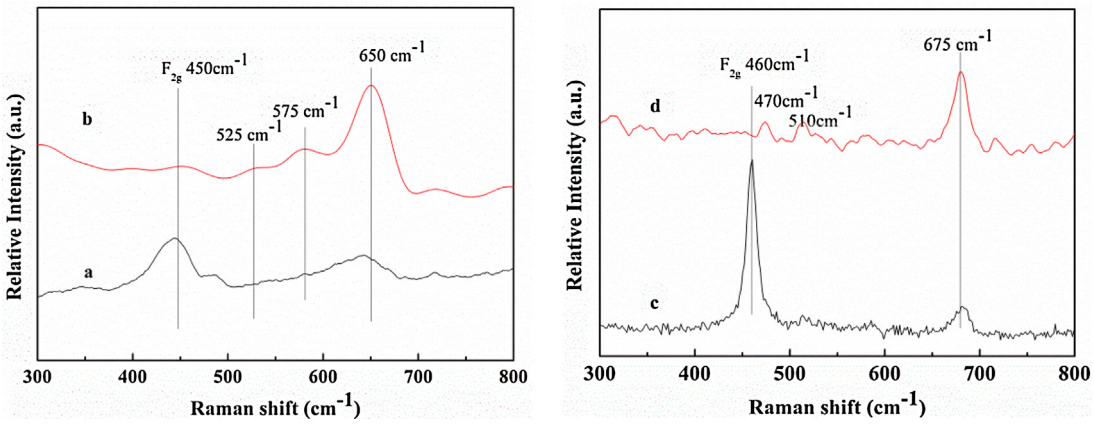

Fig. 2. Raman spectra of catalysts (a) Ru-Mn-Ce; (b) Ru-Mn-Ce (500); (c) Ru-Co-Ce; (d) Ru-Co-Ce (500).

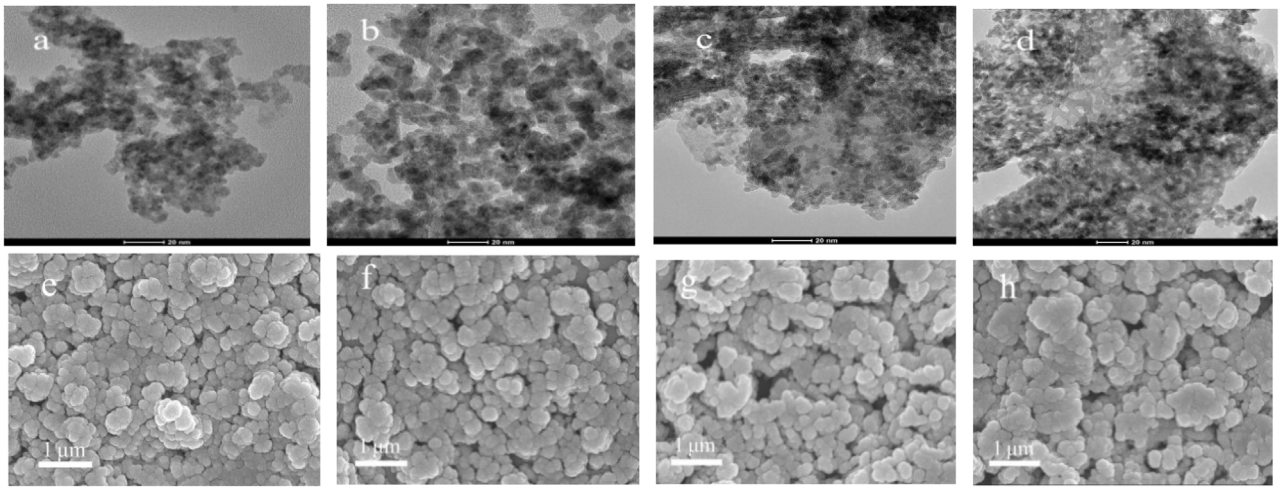

Fig. 3. TEM images of (a) Ru-Mn-Ce, (b) Ru-Mn-Ce (500), (c) Ru-Co-Ce, (d) Ru-Co-Ce (500) catalysts and SEM images of (e) Ru-Mn-Ce, (f) Ru-Mn-Ce (500), (g) Ru-Co-Ce, (h) Ru-Co-Ce (500) catalysts.

Table 1
Characterization results for Ru-Mn-Ce and Ru-Co-Ce catalysts in the present study.

Catalyst	BET SA (m^2/g)	H_2 consumption (cm^3/g)	Ru $3p_{3/2}$ (eV)	Mn $2p_{3/2}$ (eV)	Co $2p_{3/2}$ (eV)		Reduction temperature/°C		
							RuO_2	MnOx	CoOx
Mn-Ce	76.2	30.1 (4.8 + 25.3)	/	/	/		/	201 385	/
Ru-Mn-Ce	84.7	101.8 (3.2 + 57.7 + 40.9)	462.8	639.7 641.5 644.2	/		80	122 240	/
Ru-Mn-Ce (300)	61.8	89.3 (2.9 + 39.6 + 46.8)	462.6	639.7 641.5 643.8	/		100	135 285	/
Ru-Mn-Ce (500)	37.9	61.0 (2.7 + 58.3)	462.0	640.6 644.5	/		127	205	/
Co-Ce	68.5	103.3 (21.5 + 81.8)	/	/	/		/	/	195 300
Ru-Co-Ce	76.7	167.7 (5.9 + 41.2 + 120.6)	462.5 465.3	/	778.5	782.3	105	/	153 237
Ru-Co-Ce (300)	62.4	152.2 (5.6 + 38.9 + 107.7)	462.9	/	778.8 782.5		106	/	149 229
Ru-Co-Ce (500)	58.4	137.8 (6.4 + 34.8 + 96.6)	462.9	/	778.7 781.5		113	/	143 247

treatment. For Ru-Co-Ce catalysts shown in Fig. 1(e–h), the peaks corresponding to the CeO_2 are more obvious than their Ru-Mn-Ce partners, the diffraction peaks at $2\theta = 20.2$, 38.9, 50.6 and 65.3° could be assigned to CoO(OH) (JCPDS: 07-0169). With calcination, the CoO(OH) phase vanishes and a new Co_3O_4 phase appears, with corresponding diffraction peaks at 31.3, 36.9, 59.4 and 65.2° (JCPDS: 42-1467), however, the isolation of RuO_2 phase is not obvious.

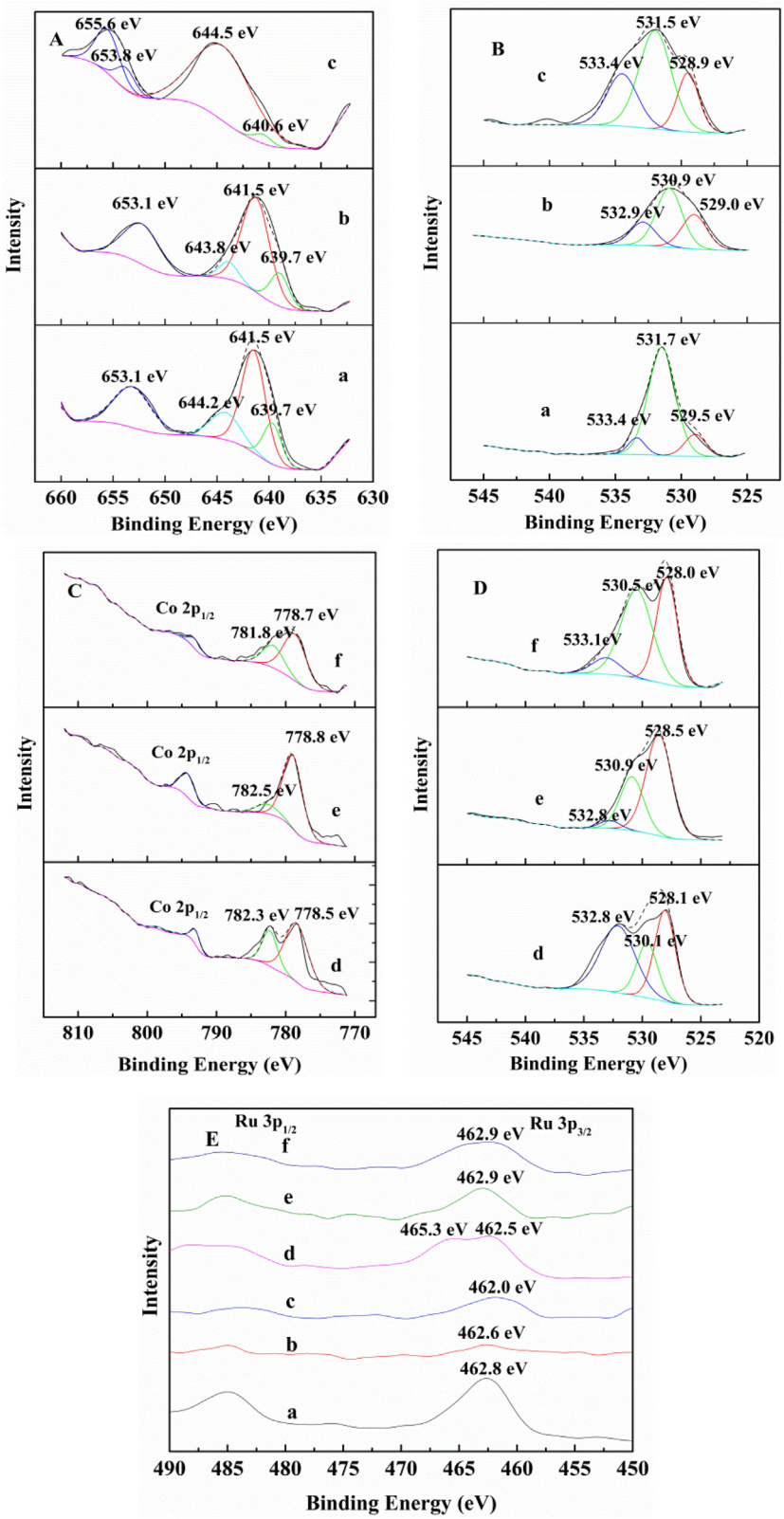

Fig. 4. XPS spectra of (A) Mn 2p, (B) O 1s of catalysts (a) Ru-Mn-Ce, (b) Ru-Mn-Ce (300), (c) Ru-Mn-Ce (500); (C) Co 2p, (D) O 1s of catalysts (d) Ru-Co-Ce, (e) Ru-Co-Ce (300), (f) Ru-Co-Ce (500); (E) Ru 2p of (a) Ru-Mn-Ce, (b) Ru-Mn-Ce (300), (c) Ru-Mn-Ce (500), (d) Ru-Co-Ce, (e) Ru-Co-Ce (300) and (f) Ru-Co-Ce (500) catalysts.

Fig. 2 shows the Raman spectra of Ru-Mn-Ce and Ru-Co-Ce catalysts before and after calcination. The 450 cm^{-1} peak corresponds to the F_{2g} Raman active mode of CeO_2 fluorite structure, due to the asymmetric breathing mode of the oxygen atoms around Ce^{4+} cations. This signal is markedly weaker for the catalyst calcined at 500 °C. None of the catalysts present any Raman peaks at 600 cm^{-1}, suggesting the ceria is low in oxygen defects [16,17]. Two peaks located at 575 and 650 cm^{-1} are present due to MnO_2, and there

is an obvious increase in peak intensity when the catalyst was calcined at 500 °C [18]. A signal at 525 cm^{-1} for Ru-Mn-Ce (500) catalysts, corresponding to the E_g Raman active mode of RuO_2 crystals, suggests the formation of a RuO_2 phase [19]. For Ru-Co-Ce catalysts shown in Fig. 2(c–d), the F_{2g} Raman active mode of the CeO_2 fluorite structure appears in the uncalcined catalysts and disappears after calcination to 500 °C. The signals at 470, 510 and 675 cm^{-1} are attributed to the spinel structure of Co_3O_4 [20].

Fig. 3 shows TEM and SEM images of Ru-Mn-Ce and Ru-Co-Ce catalysts before and after calcination. All the samples have platelet morphologies with 200 nm sizes on average, with relatively low aggregation. Both TEM and SEM images do not reveal a significant difference before and after calcination for the morphology of these four catalysts (Fig. 3a–h), although their phases segregate. The size changes of Ru species are not obvious (black flakes), which maintained at 5–8 nm before and after calcination. Meanwhile, the dispersion of Ru, Mn (Co), Ce and O atoms in the catalyst was analyzed by STEM-elemental mapping (Fig. S1–S4). The mapping of catalysts before calcination indicated that each of the Ru, Mn (Co) and O species were homogeneously dispersed. When the Ru-Mn-Ce and Ru-Co-Ce catalysts were calcined, the elemental dispersion changed, with the concentration of Ce strengthening and concentrations of Ru and Mn decreasing for Ru-Mn-Ce (500). In the cobalt-containing samples, the concentration of Ce decreased and concentrations of Ru and Co increased. This might be attributed to their different interactions when the phases changed (See XPS Ru 2p section).

For both material systems the BET surface area decreases slightly after calcination. The BET surface areas of Ru-Mn-Ce and Ru-Mn-Ce (500) are 85 and 38 m^2/g, respectively, and the Ru-Co-Ce and Ru-Co-Ce (500) show surface areas of 77 and 58 m^2/g, respectively, this shows the Ru-Co-Ce catalysts have better resistance to high temperature calcination. Fig.S5 shows the nitrogen adsorption-desorption isotherms of the four catalysts, all of which are Type H3 hysteresis loops, which are attributed to the aggregation of nanoparticles giving rise to slit-shaped pores [21].

Fig. 4 shows the XPS spectra of Ru-Mn-Ce and Ru-Co-Ce catalysts before and after calcination. Deconvolution peak fitting was performed on Mn $2p_{3/2}$ spectra aiming to determine the characteristic peaks of Mn species (Fig. 4A), including surface Mn^{2+} (639.8–640.8 eV), Mn^{3+} (641.8–642.3 eV) and Mn^{4+} (644.0–644.5 eV) [22]. For the Ru-Mn-Ce catalyst, the spectrum of Mn 2p is one asymmetrical signal which can be decomposed into three components at BE = 639.7, 641.5 and 644.2 eV which are assigned to the surface Mn^{2+}, Mn^{3+}, Mn^{4+} species, with Mn^{3+} species being the main species. The content of surface Mn^{3+} was 44.0% in the Ru-Mn-Ce Catalyst as synthesized. For the sample calcined to 300 and 500 °C catalyst, the Mn was oxidized to Mn^{4+} species, with the content of surface Mn^{4+} reaching 52.2% and 73%, respectively. This result is consistent with the XRD analysis showing that MnO_2 becomes the main manganese phase after calcination. The Co 2p peaks appear at 778.5 and 782.3 eV are corresponding to a significant amount of Co^{2+} or Co^{3+} for Ru-Co-Ce catalysts (Fig. 4C), the valence state of the cobalt remained almost unchanged after calcination. It has a 1.5 eV negative shift comparing with the 780.0 eV reported for Ru/Co_3O_4 catalyst in the literatures [23,24], which indicates a strong interaction between the Ru-Co-Ce oxides.

The spectra of O 1s of Ru-Mn-Ce and Ru-Mn-Ce (500) catalysts are described in Fig. 4B. XPS of oxygen species are complicated for mixed oxides, and peaks are generally deconvoluted into contributions from surface lattice oxygen (O_{latt}, O^{2-}), adsorbed oxygen (O_{ads}, O^{2-}, O_2^{2-}, or O^-), and adsorbed OH groups or molecular water on the surface of the catalysts (O_{sur}). The O 1 s spectra at BE = 528.0–529.5, 530.0–531.9, 532.8–534.6 eV are assigned to O_{latt}, O_{ads}, and O_{sur} species [25,26], respectively. For Ru-Mn-Ce, Ru-Mn-Ce (300) and Ru-Mn-Ce (500) catalysts (Fig. 4D), the O 1s spectra can be fit with three components and the content of O_{ads} was 79.3, 50.9 and 42.6%, respectively (the content decreased after calcination). The content of O_{ads} was lower in the cobalt containing catalysts, with 21.3, 31.5 and 57.6% for Ru-Co-Ce, Ru-Co-Ce (300) and Ru-Co-Ce (500) catalysts (the contents increased after calcination). Typically, a higher O_{ads} concentration is considered beneficial for improving catalytic performance as the surface adsorbed oxygen can attack an organic molecule [27].

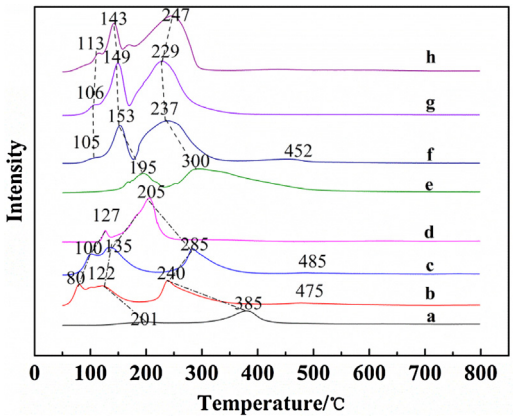

Fig. 5. H_2-TPR profiles of (a) Mn-Ce, (b) Ru-Mn-Ce, (c) Ru-Mn-Ce (300), (d) Ru-Mn-Ce (500), (e) Co-Ce, (f) Ru-Co-Ce, (g) Ru-Co-Ce (300) and (h) Ru-Co-Ce (500) catalysts.

XPS analysis of the Ru component of the catalysts (Fig. 4E) is performed on the Ru $3p_{3/2}$ located near 462.5 eV. For the Ru-Co-Ce catalyst, the peak due to Ru $3p_{3/2}$ is composed of two doublets (462.5 and 465.3 eV) with the former 1.0 eV higher than that of bulk Ru (0) (461.5 eV), suggesting RuO_2 is the dominant species [28]. The peak centered at 466.5 eV can be assigned to $RuO_2 \cdot xH_2O$ [29], while the Ru $3p_{3/2}$ peak at 465.8 eV disappears and 462.5 eV together moves to 462.9 eV for Ru-Co-Ce (300) and Ru-Co-Ce (500) catalyst, which suggests stronger interactions exist between the RuO_2 and Co_3O_4-CeO_2 mixed oxides after calcination. For the Ru-Mn-Ce, Ru-Mn-Ce (300) and Ru-Mn-Ce (500) catalysts, the BEs of Ru $3p_{3/2}$ shifted gradually from 462.8 to 462.0 eV, and intensity of the peak is weaker, it is because that the manganese species transforms from Mn^{3+} to Mn^{4+}, and part of electrons flows to ruthenium species, thus the interactions between the RuO_2 and Mn-Ce mixed oxides weaken when the Mn_3O_4 phase transforms to MnO_2 and then MnO_2 phase is isolated. Therefore, the BE of Ru $3p_{3/2}$ at 462.8–462.9 eV should be due to the strong interactions between the RuO_2 and other mixed oxides.

TPR experiments were carried out in order to study the redox properties of Mn-Ce, Co-Ce mixed oxides and corresponding Ru-Mn-Ce and Ru-Co-Ce catalysts calcined at different temperatures (Fig. 5). The temperature at peak maximum and the integral H_2 consumption in the temperature range 50–800 °C is summarized in Table 1. The peak under 150 °C is assigned to the reduction of RuO_2 to Ru^0 [29], however, the peak is not obvious, which is might be due to its low content. The main reduction peaks of ceria appear between 290 and 465 °C [30] (this peak is not obvious in our catalysts) and the peak at 205–385 °C should be assigned to the reduction of MnOx [31] (Fig. 5a–d). It is known cobalt-oxide reduction occurs in two steps-Co^{3+} to Co^{2+}, between 200 and 300 °C, and from Co^{2+} to Co^0 at 325 °C [32]. For our Ru-Co-Ce catalysts, the reduction temperature of the former decreased from 153 to 143 °C and the latter decreased from 300 to 247 °C with increasing calcination temperature (Fig. 5e–h), obviously, the reduction temperature shifted to a lower temperature as compared to pure Co_3O_4 [24], indicating that the addition of Ru markedly facilitated

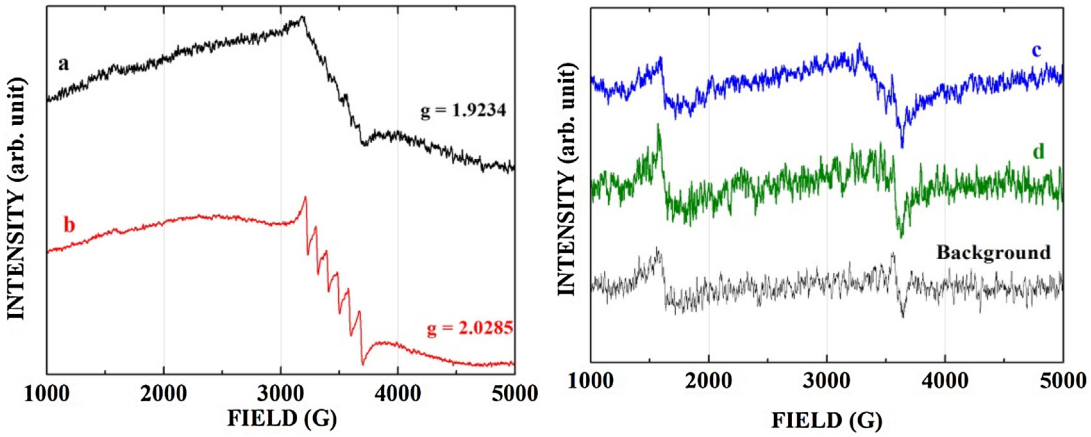

Fig. 6. EPR spectra of samples at 300 K (a) Ru-Mn-Ce, (b) Ru-Mn-Ce (500), (c) Ru-Co-Ce and (d) Ru-Co-Ce (500) catalysts.

Table 2
Aerobic oxidation of benzyl alcohol over different catalysts. [a]

Entry	Catalyst	Solvent	Conversion[b](%)	Benzaldehyde Selectivity (%)[b]
1	Ru-Mn-Ce	Benzotrifluoride	100	100
2	Ru-Mn-Ce (300)	Benzotrifluoride	66.4	100
3	Ru-Mn-Ce (500)	Benzotrifluoride	19.4	100
4	Ru-Co-Ce	Benzotrifluoride	78.2	100
5	Ru-Co-Ce (300)	Benzotrifluoride	88.4	100
6	Ru-Co-Ce (500)	Benzotrifluoride	92.3	100
7	Ru-Mn-Ce	Toluene	96.1	100
8	Ru-Mn-Ce	N,N-dimethylformamide	27.9	100
9	Ru-Mn-Ce	Dimethyl sulfoxide	38.5	100
10	Ru-Mn-Ce	Acetonitrile	10.8	100
11	Mn-Ce	Benzotrifluoride	4.6	100
12	Co-Ce	Benzotrifluoride	7.2	100
13	Ru-Co_3O_4	Benzotrifluoride	57.2	100
14	Ru-CeO_2	Benzotrifluoride	44.8	100
15	Ru-MnO_2	Benzotrifluoride	44.6	100

[a] Reaction conditions: catalyst 0.05 g (Ru: 0.03 mmol), benzyl alcohol 4 mmol, solvent 5 mL, oxygen balloon, 60 °C, 6 h.
[b] Determined by GC.

the reduction of cobalt species. For our Ru-Mn-Ce catalysts, the reduction peaks at 122–285 °C should be due to the reduction of MnO_2 to Mn_3O_4 and the reduction peaks at 240–385 °C should be due to the reduction of Mn_3O_4 to MnO, the reduction temperatures shifted to a lower temperature after RuO_2 mixed with Mn-Ce oxides, this indicates that the addition of Ru markedly facilitates the reduction of manganese species. The peaks for Mn-Ce, Ru-Mn-Ce, and Ru-Mn-Ce (300) are very weak; this shows the MnO_2 phase is less present in these catalysts. However, when the catalyst was calcined at 500 °C, a high reduction peak appeared at 205 °C, this indicates that MnO_2 has become the dominant phase in Ru-Mn-Ce (500) catalyst, which is in agreement with other data [31]. Meanwhile, the reduction peaks of RuO_2 phase changed from 80 to 127 °C for Ru-Mn-Ce catalysts and from 105 to 113 °C for Ru-Co-Ce catalysts with the increasing calcination temperature, respectively. Over all, whether they are Ru-Co-Ce or Ru-Mn-Ce catalysts, the reduction temperature increases with the higher calcination temperature, obviously, this experiment highlights different interactions between the components in mixed oxides, which results in shifting of the reduction peaks. The stronger the interaction between the oxides, the higher the initial temperature of reduction [33,34]. Differently, as the MnO_2 phase was isolated for Ru-Mn-Ce (500) catalyst, the interaction between the mixed oxides weakened. H_2 consumption significantly increased when RuO_2 mixed with Co-Ce or Mn-Ce oxides. For the Ru-Mn-Ce catalysts, the H_2 consumption decreased significantly with the increase of the calcination temperature, while the decrease of H_2 consumption was moderate with the higher calcination temperature for the Ru-Co-Ce catalysts. The decreased H_2 consumption for Ru-Mn-Ce catalysts after calcination may be due to reduced content of adsorbed oxygen. The experimental results support the theory we have proposed of the interactions change between ruthenium oxides and Co (Mn)-Ce mixed oxides before and after calcination in this system.

The transformation of phases after calcination also can be approved by EPR spectra. As seen from Fig. 6, the sextet of hyperfine lines of higher amplitude arises from Mn^{4+} species for Ru-Mn-Ce (500) catalyst [35], which further testify that the MnO_2 phase segregates from the composite after calcination. However, we cannot find the obvious signal of any Co^{2+}/Co^{3+} species for Ru-Co-Ce (500) catalyst; this illustrates no change of lone pair electron after calcination.

3.2. Catalyst activity

The oxidation of benzyl alcohol was examined as a model reaction over the four catalysts (Table 2). The Ru-Mn-Ce catalyst gave 100% conversion initially, however the activity decreases to only 19.4% when the Ru-Mn-Ce catalyst was replaced by Ru-Mn-Ce (500). The Ru-Co-Ce catalyst gave 78.2% conversion initially, which they improved to 92.3% when the calcined catalyst (500) was used (entries 1–6, Table 2). A solvent study was run using different solvents including toluene, *N*, *N*-dimethylformamide, dimethyl sulfoxide, acetonitrile, and benzotrifluoride (entries 7–10, Table 2). Of

Table 3
Aerobic oxidation of different alcohols catalyzed by Ru-Mn-Ce catalyst.[a]

Entry	Time (h)	Substrate	Product	Conversion (%)[b]	Yield (%)[b]
1	4			100	100
2[c]	4			98	98
3	3			100	100
4	0.5	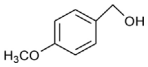	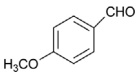	100	100
5	1	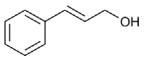	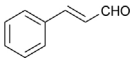	96	96
6	4			98	98
7	2	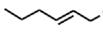		100	100
8	20	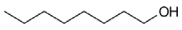	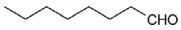	87	87
9	10	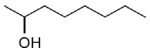	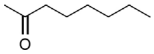	98	98
10	1			92	92
11	10	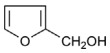		90	90
12	18	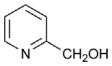		52	52
13	12			92	92

[a] Reaction conditions: catalyst 0.3 g (Ru: 0.2 mmol), alcohol 4 mmol, benzotrifluoride 5 mL, oxygen balloon, 60 °C.
[b] Determined by GC.
[c] Recycled test (5th).

these reaction media tested, benzotriflouride performed the best of the studied reaction solvents, and was used in further tests.

To study the role of Ru, Mn-Ce and Co-Ce mixed oxides were prepared by the same procedure, and the reaction yielded 4.6% and 7.2% conversion of benzyl alcohol, respectively (entries 11–12, Table 2). This indicated that the Ru component was responsible for the catalytic activity. To further illustrate the mixed-oxide dependence on activity, binary Ru-Co_3O_4, Ru-CeO_2 and Ru/MnO_2 catalysts were prepared under the same conditions (entries 13–15, Table 2), and these systems gave 57.2%, 44.8% and 44.6% conversion of benzyl alcohol. This suggests that the use of binary oxides in addition to the ruthenium component yield a high oxidative catalytic activity than the single component alone.

To further understand catalytic activity, the oxidation of various alcohols was examined over the Ru-Mn-Ce catalyst using benzotrifluoride as solvent at 60 °C, and the results are shown in Table 3. All the benzylic and allylic alcohols show high yields for the oxidative dehydrogenation (entries 1–7, Table 3), transforming to the corresponding aldehydes in higher than 96% yield. The primary aliphatic alcohols were readily oxidized to aldehydes in high yields with a longer reaction time, and aliphatic secondary alcohols had higher catalytic performance than the primary ones, which shows the promotion of the electron density of substrates in this reaction (entries 8–9, Table 3). When the Ru-Mn-Ce catalysts were used in the oxidation of heterocyclic alcohols, thiophene-2-methanol, and furan-2-methanol could be oxidized to corresponding aldehyde in short time, but pyridine-2-methanol showed low reactivity for oxidative dehydrogenation, reaching only 52% yield with an 18 h reaction time (entries 10–12, Table 3). Cyclohexanol was effectively oxidized to cyclohexanone in 12 h (entry 13, Table 3). To demonstrate recyclability of the catalyst, the catalyst was used sequentially in five reactions and the Ru-Mn-Ce catalyst gave 98% yield for the fifth use. Leaching of Ru was tested by hot filtration, and induced coupled plasma techniques (ICP) revealed no ruthenium in the filtrate.

4. Discussion

The Ru-Mn-Ce catalysts showed poor performance after they were calcined, while Ru-Co-Ce catalysts showed better performance after they were calcined. For Ru-Mn-Ce catalysts, the obvious loss of catalytic property is due to the change of phase. All characterization techniques showed that the Mn_3O_4 phase was transformed to MnO_2 after the Ru-Mn-Ce catalyst was calcined at 500 °C, and this change of Mn valence results in a more loose distribution (Fig.S1, S2). Through the formation of Mn-Ce mixed oxides by the addition of Ce, a synergistic interaction between Mn and Ce oxides can be interpreted as an oxygen transfer mechanism. CeO_2 may act as an oxygen reservoir, transferring oxygen from the oxygen atmosphere to the Ru and MnO_x, which realizes the effective activation of molecular oxygen [36,37]. However, this transfer of oxygen is based on good-conditional Mn-Ce mixed oxides as a pre-condition; we propose this oxygen transfer mechanism has been blocked when MnO_2 segregates from the composite due to increased valence [38], this segregation also can be approved by EPR and TPR data.

For Ru-Co-Ce catalysts, the increase of catalytic activity is due to the change of the crystalline phase of cobalt. All characterization techniques (XRD, Raman and XPS) show CoO(OH) was transformed to Co_3O_4 after the Ru-Co-Ce catalyst was calcined at 500 °C. The

change of Co valence leads to a denser distribution (Figs. S3, S4) opposite to the Ru-Mn-Ce catalysts, and stronger interactions were obtained when the CoO(OH) phase was transformed to Co_3O_4. This may strengthen synergistic interactions between Co and Ce oxides (approved by the XPS and TPR test), further enhancing the oxygen transfer mechanism. This conclusion also can be drawn from the XPS O 1s data, as the contents of O_{ads} for Ru-Mn-Ce catalysts decrease after calcination, which may block oxygen transfer, while the contents of O_{ads} for Ru-Co-Ce and Ru-Co-Ce (500) catalysts alternatively increase and intensify the oxygen transfer.

From the reaction results, the activity is principally due to the RuO_2, as evidenced by the lower conversions of the ruthenium-free mixed oxides. The activation and transfer of molecular oxygen to the ruthenium is likely due to the mixed oxides in the composite. Highly dispersed RuO_2 nanocrystals agglomerated due to high-temperature calcination whether for Ru-Mn-Ce (500) or Ru-Co-Ce (500) catalyst; however, the results obtained from them are different. This difference is mainly due to phase separation of the former leading to blockage of oxygen transfer and the agglomeration of RuO_2 is not obvious even if the catalyst is calcined (Figs. S2 and S4). This different phase separation also can be approved by the change of BET surface area and H_2 consumption when all the catalysts are calcined.

5. Conclusions

Two kinds of ternary mixed oxides, Ru-Mn-Ce and Ru-Co-Ce, were prepared by a co-precipitation method and used in the aerobic oxidation of alcohols to their corresponding aldehydes (ketones). Based on the characterization data, the interactions between ruthenium oxides and Mn-Ce mixed oxides weakened, while the opposite was observed in the cobalt-containing system after they were calcined. The decreased interactions between Mn-Ce and ruthenium (oxide) decreased the content of adsorbed oxygen and blocked oxygen transfer, while the heat treatment of the Ru-Co-Ce catalyst increased the content of adsorbed oxygen and promoted oxygen transfer. Under optimal reaction conditions, various kinds of alcohols were oxidized with high yields over Ru-Mn-Ce catalyst. The results also showed ruthenium oxide dispersed in the mixed oxides plays a key role in this reaction. The interactions between Ru oxide and Mn-Ce oxides as well as the higher concentration of adsorbed oxygen are especially important in the catalytic performance of these catalysts.

Acknowledgements

This work is financially supported by the National Natural Science Foundation of China (21303085), the Natural Science Foundation of Jiangsu Province (BK20130901, BK20130930), the Jiangsu Government Scholarship for Overseas Studies (JS-2014040, JS-2014060), the Program to Cultivate Outstanding Young Key Teachers of Nanjing Normal University and the Priority Academic Program Development of Jiangsu Higher Education Institutions. SLS acknowledges the support of the US Department of Energy, Office of Basic Energy Sciences, Division of Chemical, Biological and Geological Sciences under grant DE-FG02-86ER13622.A000.

References

[1] L.M.D.R.S. Martins, A.P.C. Ribeiro, S.A.C. Carabineiro, J.L. Figueiredoc, A.J.L. Pombeiro, Dalton Trans. 45 (2016) 6816–6819.
[2] G.-J. ten Brink, I.W.C.E. Arends, R.A. Sheldon, Science 287 (2000) 1636–1639.
[3] D. Enache, et al., Science 311 (2006) 362–365.
[4] K. Yamaguchi, K. Mori, T. Mizugaki, K. Ebitani, K. Kaneda, J. Am. Chem. Soc. 122 (2000) 7144–7145.
[5] K. Mori, T. Hara, T. Mizugaki, K. Ebitani, K. Kaneda, J. Am. Chem. Soc. 126 (2004) 10657–10666.
[6] H. Wang, W. Fan, Y. He, J. Wang, J.N. Kondo, T. Tatsumi, J. Catal. 299 (2013) 10–19.
[7] J. Liu, F. Wang, Z. Gu, X. Xu, Chem. Eng. J. 151 (2009) 319–323.
[8] S. Sajip, J.K. Bartley, A. Burrows, M.T.S. Schulz, A. Tuel, J.C. Volta, C.J. Kiely, G.J. Hutchings, New J. Chem. 25 (2001) 125–130.
[9] W. Zhan, Y. Guo, Y. Wang, X. Liu, Y. Guo, Y. Wang, Z. Zhang, G. Lu, J. Phys. Chem. B 111 (2007) 12103–12110.
[10] X. Tang, J. Li, J. Hao, Catal. Commun. 11 (2010) 871–875.
[11] B. Qiao, A. Wang, M. Takahashi, Y. Zhang, J. Wang, Y. Deng, T. Zhang, J. Catal. 279 (2011) 361–365.
[12] E.M. Slavinskaya, R.V. Gulyaev, A.V. Zadesenets, O.A. Stonkus, V.I. Zaikovskii, Yu. V. Shubin, S.V. Korenev, A.I. Boronin, Appl. Catal. B: Environ. 166–167 (2015) 91–103.
[13] Z. Miao, Y. Zhang, X. Pan, T. Wu, B. Zhang, J. Li, T. Yi, Z. Zhang, X. Yang, Catal. Sci. Technol. 5 (2015) 1314–1322.
[14] P. Zhang, H. Lu, Y. Zhou, L. Zhang, Z. Wu, S. Yang, H. Shi, Q. Zhu, Y. Chen, S. Dai, Nat. Commun. 6 (2015) 8446.
[15] J. Gaálová, P. Topka, L. Kaluža, O. Šolcová, Catal. Today 175 (2011) 231–237.
[16] L. Ma, D. Wang, J. Li, B. Bai, L. Fu, Y. Li, Appl. Catal. B: Environ 148–149 (2014) 36–43.
[17] W.Y. Hernandez, M.A. Centeno, F. Romero-Sarria, J.A. Odriozola, J. Phys. Chem. C 113 (2009) 5629–5635.
[18] C. Julien, M. Massot, R. Baddour-Hadjean, S. Franger, S. Bach, J.-P. Pereira-Ramos, Solid State Ionics 159 (2003) 345–356.
[19] A. Korotcov, H.P. Hsu, Y.S. Huang, D.S. Tsai, K.K. Tiong, Crystal Growth Des. 6 (2006) 2501–2506.
[20] M. Rashad, M. Rüsing, G. Berth, K. Lischka, A. Pawlis, J. Nanomater. 714853 (2013) 1–6.
[21] K.S.W. Sing, Pure Appl. Chem. 54 (1982) 2201–2218.
[22] H. Li, D. Zhang, P. Maitarad, L. Shi, R. Gao, J. Zhang, W. Cao, Chem. Commun. 48 (2012) 10645–10647.
[23] F. Li, J. Chen, Q. Zhang, Y. Wang, Green Chem. 10 (2008) 553–562.
[24] C. Wang, C. Zhang, W. Hua, Y. Guo, G. Lu, S. Gil, A.G. Fendler, RSC Adv. 6 (2016) 99577–99585.
[25] A.F. Carley, M.W. Roberts, A.K. Santra, J. Phys. B: Chem. 101 (1997) 9978–9983.
[26] L.F. Liotta, F. Puleo, V. La Parola, S.G. Leonardi, N. Donato, D. Aloisio, G. Neri, Electroanalysis 27 (2015) 684–692.
[27] S. Rousseau, S. Loridant, P. Delichere, A. Boreave, J.P. Deloume, P. Vernoux, Appl. Catal. B: Environ. 88 (2009) 438–447.
[28] Y. Okawa, T. Masuda, H. Uehara, D. Matsumur, K. Tamur, Y. Nishihatad, K. Uosaki, RSC Adv. 3 (2013) 15094–15101.
[29] N. Zhang, Y. Du, M. Yin, C. Guan, J. Feng, D. Li, RSC Adv. 6 (2016) 49588–49596.
[30] L.F. Liotta, G. Di Carlo, G. Pantaleo, A.M. Venezia, G. Deganello, Appl. Catal. B. Environ. 66 (2006) 217–227.
[31] C. Zhou, F. Peng, H. Wang, H. Yu, J. Yang, X. Fu, Fuel Cells 11 (2011) 301–308.
[32] P. Gawade, B. Bayram, A.M.C. Alexander, U.S. Ozkan, Appl. Catal. B Environ. 128 (2012) 21–30.
[33] Y. Ji, Z. Zhao, A. Duan, G. Jiang, J. Liu, J. Phys. Chem. C 113 (2009) 7186–7199.
[34] T.M. Sankaranarayanan, A. Berenguer, C. Ochoa-Hernández, I. Moreno, P. Jana, J.M. Coronado, D.P. Serranoa, P. Pizarro, Catal. Today 243 (2015) 163–172.
[35] A.G. Badalyan, P.P. Syrnikov, C.B. Azzoni, P. Galinetto, M.C. Mozzati, J. Rosa, V.A. Trepakov, L. Jastrabik, J. Appl. Phys. 104 (2008) 033917.
[36] G. Qi, R.T. Yang, J. Chem. Soc. Chem. Commun. 84 (2003) 8–849.
[37] X. Tang, Y. Li, X. Huang, Y. Xu, H. Zhu, J. Wang, W. Shen, Appl. Catal. B: Environ. 62 (2006) 265–273.
[38] Z. Ding, L. Li, D. Wade, E.F. Gloyna, Ind. Eng. Chem. Res. 37 (1998) 1707–1716.